Pure Appl. Chem., Vol. 73, No. 11, pp. 1689–1703, 2001.

Theories of structural and dynamic properties of ions in discrete solvents. Application to magnetic resonance imaging*

Pascal H. Fries[1,‡], Johannes Richardi[1], Sebastian Rast[1], and Elie Belorizky[2]

[1]Laboratoire de Reconnaissance Ionique, Service de Chimie Inorganique et Biologique (UMR 5046), Département de Recherche Fondamentale sur la Matière Condensée, CEA-Grenoble, 17, rue des Martyrs, F-38054, Grenoble Cedex 9, France; [2]Laboratoire de Spectrométrie Physique, CNRS-UMR 5588, Université Joseph Fourier, B.P. 87, F-38402, St Martin d'Hères Cedex, France

Abstract: The molecular Ornstein–Zernike (MOZ) formalism used to compute the structure of a liquid solution is briefly presented. Its ability to describe the equilibrium properties of aprotic solvents and of their electrolyte solutions is demonstrated from selected examples. The potential of mean force and the relative motion of ions in water are studied by the powerful method of intermolecular nuclear magnetic relaxation dispersion (NMRD) in paramagnetic solutions. The interest of the ion–ion dynamics in medical magnetic resonance imaging (MRI) is shown by a typical NMRD study involving paramagnetic gadolinium Gd^{3+} complexes.

INTRODUCTION

Among the numerous applications of chemical thermodynamics, the description of electrolyte solutions has generated a vast literature [1] because of their practical interest and the fundamental challenge to correlate solution properties with the very discrete nature of strongly interacting ions and solvent molecules. We present recent advances in the statistical mechanics of liquids, which, thanks to modern computers, make it possible to rapidly calculate a structure of solution, i.e., the equilibrium distribution of the different species, at least at the two-particle level. In the second section, we briefly recall the molecular Ornstein–Zernike (MOZ) formalism [2–5], which we use to compute the liquid structure and which can be a very fast alternative to simulations. The third section demonstrates the accuracy of the hypernetted chain (HNC) approximation of the MOZ theory for electrolyte solutions in aprotic solvents. In the fourth section, we study the relative distribution and motion of ions in paramagnetic aqueous solutions by nuclear magnetic relaxation dispersion (NMRD). Particular care is taken to present the main concepts required to interpret the experiment. How such an investigation can help to characterize the efficiency of Gd^{3+} chelates for medical magnetic resonance imaging (MRI) is also shown. Finally, the context of the present work and promising future developments are discussed in the fifth section.

*Plenary lecture presented at the 27th International Conference on Solution Chemistry, Vaals, The Netherlands, 26–31 August 2001. Other presentations are published in this issue, pp. 1679–1748.

‡Corresponding author

Dedicated to the memory of Prof. H. G. Hertz.

INTEGRAL EQUATION FORMALISM

Consider a general liquid mixture [2–6] made of neutral and charged anisotropic molecules of species indexed by A, B, X…. The system is characterized by the set of direct intermolecular potentials $U_{AB}(12)$ *in vacuo* and by the numerical densities ρ_X of the various species X, i.e., the number of X molecules per volume unit. Denote the coordinates of position and orientation of a molecule by numbers such as 1, 2, 3. The total correlation function $h_{AB}(12)$ between two molecules of A and B species, of coordinates 1 and 2, is defined as

$$h_{AB}(12) \equiv g_{AB}(12) - 1 \tag{1}$$

and represents the deviation of the A/B pair distribution function $g_{AB}(12)$ from the uniform distribution value 1, which corresponds to a structureless continuum. The function h_{AB} contains all the statistical structural information on the spatial correlations of two molecules of species A and B due to their direct intermolecular potential $U_{AB}(12)$ *in vacuo* and to their interactions with the neighboring molecules. The set of functions $h_{AB}(12)$ describes the liquid structure at the two-particle level.

The integral equation approximations rest on the judicious splitting of each function $h_{AB}(12)$ into the so-called direct and indirect correlation functions $c_{AB}(12)$ and $\eta_{AB}(12)$ as

$$h_{AB}(12) \equiv c_{AB}(12) + \eta_{AB}(12) \tag{2}$$

where $c_{AB}(12)$ and $\eta_{AB}(12)$ are the numerical solutions of the following system of coupled equations:

(i) the Ornstein–Zernike (OZ) convolution relations

$$\eta_{AB}(12) = \frac{1}{8\pi^2} \sum_{\text{species X}} \rho_X \int c_{AX}(13)\left[c_{XB}(32) + \eta_{XB}(32)\right] d3 \tag{3}$$

where $d3 = d\mathbf{R}_3 d\Omega_3$ is the elementary integration volume over the position $\mathbf{R}_3$ and the orientation Ω_3 of a molecule of species X.

(ii) the closure equations

$$c_{AB}(12) = \exp\left[-\beta U_{AB}(12) + \eta_{AB}(12) + B_{AB}(12)\right] - 1 - \eta_{AB}(12) \tag{4}$$

where $B_{AB}(12)$ is a so-called bridge function which often has simple and quite accurate approximations despite its intricate dependence on the liquid structure. For instance, within the popular hypernetted chain (HNC) approximation, we have $B_{AB}(12) = 0$. Then, there are as many OZ and closure equations as unknown functions c_{AB} and η_{AB} to be determined. The numerical solution of the HNC approximation of the present molecular Ornstein–Zernike (MOZ) theory is based on the expansion of the molecular correlation functions in series of rotational invariants [2] and can be computed by iterative algorithms [3–6].

ELECTROLYTE SOLUTIONS IN APROTIC SOLVENTS

Each intermolecular potential $U_{AB}(12)$ is described as the sum of a short-ranged site–site contribution and an electrostatic part [6–9]. The molecular polarizability is taken into account by an enhanced dipole moment calculated by a self-consistent mean field (SCMF) approach [3,6,9].

Structure of solvents

We consider unpolarizable models of acetonitrile and acetone at 298 K and of chloroform at 293 K [7,8]. In Fig. 1, typical site–site distribution functions, calculated by the MOZ-HNC approximation, are compared with Monte-Carlo (MC) and molecular dynamics (MD) simulation data. Besides slight shifts

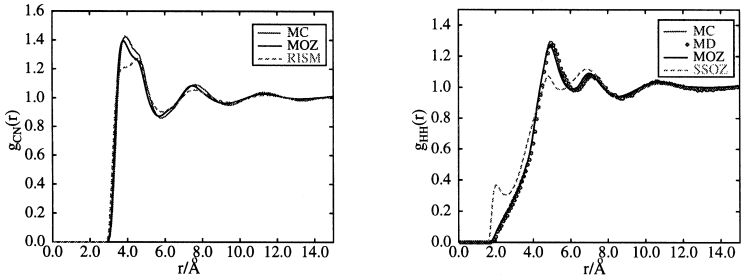

Fig. 1 (a) The carbon–nitrogen distribution functions $g_{CN}(r)$ in acetonitrile. (b) The hydrogen–hydrogn distribution function $g_{HH}(r)$ in chloroform.

to shorter distances in the positions of the first peaks, the MOZ theory is quite accurate and represents a notable progress with respect to the less complex site–site Ornstein–Zernike (SSOZ) approximation [10]. The MOZ dielectric constants ε of acetonitrile, acetone, and chloroform are 18.5, 9.2, and 2.3, and compare favorably to the simulation data 16.7, 9.0, and 2.4 to 2.6, respectively.

Ionic solvation

We study the solvation of simple alkali and halide ions in a model of polarizable acetonitrile [9] at 298 K. The MOZ-HNC approximation leads to a dielectric constant $\varepsilon = 36.4$ in very good agreement with the experimental value 35.9. A realistic value of the solvent dielectric constant is essential for a correct description of the ionic interactions in solution because it governs the long-range behavior of the ion–solvent and ion–ion correlation functions. The MOZ ion–solvent intercenter distribution function $g^{000}_{is,00}$ and the orientational correlation $\langle \cos\theta_{R\mu} \rangle$ are shown in Fig. 2 for Na^+ in acetonitrile. Each maximum in the $g^{000}_{is,00}$ function indicates a solvation shell. It is usually expected that the negative end of the solvent molecule points toward the cation, which corresponds to negative values in the $\langle \cos\theta_{R\mu} \rangle$ function. This is observed for the first and third solvation shells, whereas the solvent molecules in the second shell have an unexpected opposite orientation (see arrows in Fig. 2). Recent comparisons with the results from MC simulations show that this energetically unfavored orientation is not an artifact of the approximate HNC closure. The surprising formation of the anomalous second shell can be explained as follows. As shown in Fig. 2, it is due to the persistence of molecular antiparallel arrangements that correspond to the most probable configuration in pure liquid acetonitrile. Obviously, the solvation structure is strongly influenced by the solvent–solvent spatial correlations. This is a very general phenomenon, because it is also observed for the other ions in acetonitrile and for the solvation in acetone. Finally,

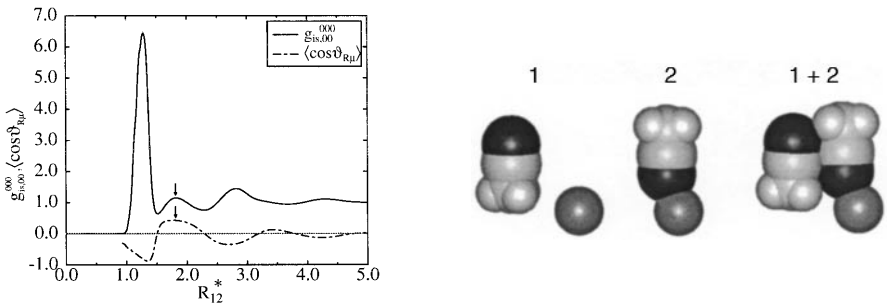

Fig. 2 (a) The intercenter distribution function $g^{000}_{is,00}$ of the Na^+/CH_3CN pair and the orientational correlation $\langle \cos\theta_{R\mu} \rangle$ between its intercenter vector and the CH_3CN electric dipole. (b) Preferential Na^+/CH_3CN and CH_3CN/CH_3CN arrangements in the solvation structure.

the MOZ Gibbs solvation energies of salts of alkali and halide ions are in good agreement with the experimental values, apart from salts including small ions.

Concentrated solution of dissociated ions

We apply the SCMF/HNC approximation of the MOZ theory to a 0.4 M solution of cryptates K^+222/ClO_4^- in deuterated acetonitrile [6]. The model of polarizable acetonitrile in the pure solvent and the theory are both justified by the excellent agreement between the MOZ intermolecular neutron-scattering cross-section I^{inter} and the experimental data [11] displayed in Fig. 3a. In the concentrated solution, the parameters defining the short-ranged intermolecular potentials involving the dissolved molecular ions cannot be easily computed by *ab initio* quantum calculations. However, the short computer time needed to calculate the numerical solution of the MOZ theory enables us to fit these parameters so as to reproduce the small-angle neutron-scattering (SANS) data shown in Fig. 3b. The various pair distribution functions, which lead to the theoretical SANS results and define the solution structure, are then justified. This structure can be analyzed and additional properties computed. This is a generalization to discrete solvents of a method widely used in the case of a dielectric continuum [1].

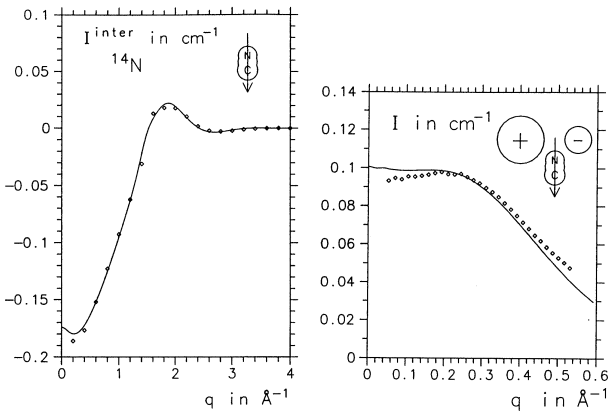

Fig. 3 (a) Intermolecular neutron-scattering cross-section I^{inter} for pure acetonitrile. (b) Total neutron-scattering intensity I for a cryptate solution in this solvent.

RELATIVE DISTRIBUTION AND MOTION OF IONS IN AQUEOUS SOLUTIONS: INTERMOLECULAR NMRD STUDIES

As early as 1953, Torrey [12] envisaged intermolecular nuclear relaxation as an investigation tool for the condensed matter. Starting at the beginning of the 1960s, Hertz *et al.* [13,14] undertook a systematic study of the liquid state by measuring the intermolecular relaxation rates of numerous nuclei on molecules and ions in a wide variety of pure solvents, liquid mixtures, and solutions. Indeed, this is a particularly suitable method for probing the relative distribution and motion of two given species.

Theory of the intermolecular nuclear relaxation in paramagnetic solutions [15–18]

The intermolecular nuclear relaxation is more easily measured and interpreted when it is due to paramagnetic solutes which are the major source of relaxation of the nuclear spins I carried by the molecules M_I. These paramagnetic solutes are either free radicals, ions of the transition group or of the rare earth group. In this article, we only consider paramagnetic molecules M_S, the moments $\mathbf{m}_e$ of which have negligible contributions from the orbital angular momenta of the electrons. These moments are

those of "pure" spins, i.e., $\mathbf{m}_e = -g_S \mu_B \mathbf{S}$ with $g_S = 2$. This is the case for free radicals, complexes of $(3d)^5$ metal ions such as Mn^{2+} and Fe^{3+}, and complexes of $(4f)^7$ lanthanides such as Gd^{3+}.

In a fixed external magnetic field B_0, the observed longitudinal and transverse relaxation rates $R_1 = 1/T_1$ and $R_2 = 1/T_2$ of a given nuclear species in the presence of solutes carrying electronic magnetic moments $\mathbf{m}_e$ are

$$R_i = R_i^0 + R_{in}^e \quad (i = 1,2), \tag{5}$$

where $R_i^0 = 1/T_i^0$ are the relaxation rates of these nuclei in the absence of any paramagnetic species (diamagnetic solution). Then, even at very low concentrations c_S in mol.L^{-1} of paramagnetic solutes carrying "pure" spins, their intermolecular interactions yield the main contributions $R_{in}^e = R_{iS} = 1/T_i^{inter}$ to the measured rates. The paramagnetic intermolecular relaxation rates R_{in}^e are essentially proportional to c_S, so that it is often convenient to introduce the relaxivities $r_i = R_{in}^e$. The paramagnetic intermolecular relaxation arises from two mechanisms: (i) the dipolar magnetic interaction between the investigated nuclear spin I and the electronic spin S; (ii) the hyperfine scalar coupling between I and S when there is some unpaired spin density of the electrons at the nucleus. Then, the total intermolecular relaxation rates are

$$\frac{1}{T_i^{inter}} = \frac{1}{T_{idip}^{inter}} + \frac{1}{T_{is}^{inter}} \quad (i = 1,2) \tag{6}$$

where $1/T_{idip}^{inter}$, $1/T_{is}^{inter}$ are the dipolar and scalar contributions, respectively. The detailed theory giving the corresponding expressions of the relaxation rates was given previously [15–18]. Let γ_I, γ_S be the gyromagnetic ratios of the I and S spins, respectively, and $\omega_I = 2\pi\nu_I = |\gamma_I| B_0$, $\omega_S = 2\pi\nu_S = |\gamma_S| B_0$ their associated Larmor angular frequencies. We have $\gamma_S >> \gamma_I$ and $\omega_S >> \omega_I$.

Dipolar intermolecular nuclear relaxation

Within the Solomon model of nuclear relaxation, which neglects the relaxation of the electronic spins, the intermolecular dipolar magnetic relaxation rates are

$$\frac{1}{T_{1\,dip}^{inter}} = \frac{2}{5}\gamma_I^2\gamma_S^2\hbar^2 S(S+1)\left[j_2(\omega_I) + \frac{7}{3}j_2(\omega_S)\right] \tag{7}$$

$$\frac{1}{T_{2\,dip}^{inter}} = \frac{2}{5}\gamma_I^2\gamma_S^2\hbar^2 S(S+1)\left[\frac{2}{3}j_2(0) + \frac{1}{2}j_2(\omega_I) + \frac{13}{6}j_2(\omega_S)\right] \tag{8}$$

where the dipolar spectral density $j_2(\omega)$ is the Fourier transform

$$j_2(\omega) = \frac{1}{2\pi}\int_{-\infty}^{+\infty} g_2(t) e^{-i\omega t} dt \tag{9}$$

of the time correlation function $g_2(t)$

$$g_2(t) = \left\langle r_{t=0}^{-3} Y_{2q}(\theta_{t=0}, \phi_{t=0}) \left[r_t^{-3} Y_{2q}(\theta_t, \phi_t) \right]^* \right\rangle \tag{10}$$

of the random functions $r^{-3}Y_{2q}(\theta,\phi)$ which define the intermolecular dipolar magnetic Hamiltonian and depend on the relative position vector $\mathbf{r}(r,\theta,\phi)$ of the interacting spins I and S. The spectral density $j_2(\omega)$ is proportional to the number density $N_S = 10^{-3} c_S N_{Avogadro}$ in cm^{-3} of the electronic spins. It is convenient to introduce the natural units of the relative translational diffusion of the two interacting molecules. The length unit is the minimal distance of approach b of the centers of these molecules approximated as hard spheres in this work. The time unit is their translational correlation time $\tau = b^2 / D$, D being their relative diffusion coefficient. Here, D is assumed to be the sum $D = D_I^t + D_S^t$ of the self-

diffusion constants D_I^t and D_S^t of the diamagnetic and paramagnetic species, respectively. Then, $j_2(\omega)$ can be expressed in terms of the reduced dipolar spectral density $\bar{j}_2(\omega\tau)$ as

$$j_2(\omega) = \frac{N_S \tau}{\pi b^3}\, \bar{j}_2(\omega\tau) \tag{11}$$

The reduced spectral density $\bar{j}_2(\omega\tau)$ also depends on the rotational diffusion constants D_I^{r} and D_S^{r} of the two species and on the eccentricity parameters $(\rho_I/b)^2$, $(\rho_S/b)^2$, where ρ_I, ρ_S are the distances of I and S to the centers of their respective molecules. It has been shown [15–18] that $\bar{j}_2(\omega\tau)$ can be expressed in a power series of these eccentricity parameters, where obviously the leading term of $\bar{j}_2(\omega\tau)$ corresponds to the situation where the spins are located at the ion centers. Then, the time correlation function $g_2(t)$ reduces to

$$G_2(t) = N_S \iint g_{IS}(R_0)\rho(\mathbf{R}_0, \mathbf{R}, t) R_0^{-3} Y_{2q}(\Theta_0, \Phi_0)\left[R^{-3} Y_{2q}(\Theta, \Phi)\right]^* d^3\mathbf{R}_0 d^3\mathbf{R} \tag{12}$$

where $\mathbf{R}_0(R_0,\Theta_0,\Phi)$ and $\mathbf{R}(R,\Theta,\Phi)$ are the intercenter vectors at time $t = 0$ and time t, respectively. The spatial correlations between the interacting species shows up in their equilibrium pair distribution function g_{IS}, also given by the Boltzmann exponential

$$g_{IS} = \exp\left[-\beta w_{IS}\right] \tag{13}$$

of their potential of mean force (PMF) w_{IS}, which is an effective thermal potential that can be obtained from the MOZ theory. The conditional probability, $\rho(\mathbf{R}_0,\mathbf{R},t)$, of finding the molecule centers at the relative position $\mathbf{R}$ at time t given that they were at $\mathbf{R}_0$ at time $t = 0$, is assumed to be the solution of the Smoluchowski generalized diffusion equation

$$\frac{\partial}{\partial t}\rho(\mathbf{R}_0, \mathbf{R}, t) = D\left\{\Delta_{\mathbf{R}}\rho(\mathbf{R}_0, \mathbf{R}, t) + \frac{1}{k_{\mathrm{B}}T}\,\mathrm{div}_{\mathbf{R}}\left[\rho(\mathbf{R}_0, \mathbf{R}, t)\mathbf{grad}_{\mathbf{R}} w_{IS}(R)\right]\right\} \tag{14}$$

with the initial condition $\rho(\mathbf{R}_0,\mathbf{R},t = 0) = \delta(\mathbf{R} - \mathbf{R}_0)$ and the hard sphere boundary condition. The numerical procedure for solving the Smoluchowski diffusion equation and calculating the spectral density $\bar{j}_2(\omega\tau)$ has been described elsewhere [15].

Equation 12 is the meeting point between the relaxation measurements and the theory of liquid solutions requiring a model for calculating the pair distribution function (13). The interpretation of the relaxation needs the Fourier transform $J_2(\omega)$ of the correlation function $G_2(t)$, and more generally the Fourier transform $j_2(\omega)$ of $g_2(t)$. As the intermolecular relaxation rates $1/T_{i\mathrm{dip}}^{\mathrm{inter}}$ depend on $j_2(\omega)$ values calculated at Larmor frequencies ω_I and ω_S, which are proportional to the field B_0, NMRD studies allow to determine $j_2(\omega)$ over a large frequency range, and thus to better characterize the relative dynamics of M_I and M_S through $g_2(t)$.

Hyperfine scalar intermolecular nuclear relaxation

The hyperfine scalar coupling between a nuclear spin I and an electronic spin S can be expressed as [15–17]

$$H_{\mathrm{s}} = \hbar A(r)\mathbf{I.S} \tag{15}$$

where the coupling function $A(r)$ is conveniently written in terms of a dimensionless quantity $a(r)$ as $A(r) = (\gamma_I\gamma_S\hbar/b^3)a(r)$. This simplifies any comparison between the magnetic dipolar and hyperfine contributions to the total intermolecular relaxation rates. Within the Solomon model of nuclear relaxation, the fluctuations of the coupling function $A(r)$ resulting from the random relative motions of the interacting spins lead to the following nuclear relaxation rates:

$$\frac{1}{T_{1\mathrm{s}}^{\mathrm{inter}}} = \frac{2\pi}{3} S(S+1)\frac{\gamma_I^2\gamma_S^2\hbar^2}{b^6}\, j_{\mathrm{s}}(\omega_S) \tag{16}$$

$$\frac{1}{T_{2s}^{inter}} = \frac{\pi}{3} S(S+1) \frac{\gamma_I^2 \gamma_S^2 \hbar^2}{b^6} \left[j_s(0) + j_s(\omega_S) \right] \tag{17}$$

where the scalar spectral density $j_S(\omega)$ is the Fourier transform of the hyperfine time correlation function $g_s(t) = \langle a(r_{t=0}) a(r_t) \rangle$.

Hyperfine coupling determination by frequency shift measurements

Contrary to the dipolar coupling, which has a well-known long-ranged dependence on the interspin vector **r**, the magnitude and spatial dependence of the short-ranged hyperfine coupling function $a(r)$ has to be determined by complementary measurements [16,19]. For each nuclear spin I of frequency, this can be done by measuring the shift $\Delta\nu = \nu - \nu_0$ of its resonance frequency ν induced by the introduction of paramagnetic solutes ν_0 in the diamagnetic zero solution. This shift arises from two contributions of the thermal averages $\langle \mathbf{m}_e \rangle$ of the magnetic electronic moments. The first one is due to the long-ranged dipolar coupling with the averages $\langle \mathbf{m}_e \rangle$ of the moments located in the whole sample and is related to demagnetizing field effects. The second one stems from the hyperfine scalar coupling with the moments very near the considered nucleus. Then, the total relative frequency shift in a paramagnetic solution reads

$$\frac{\Delta\nu}{\nu_0} = \frac{\Delta\nu_{dip}}{\nu_0} + \frac{\Delta\nu_{hyp}}{\nu_0} \tag{18}$$

The dipolar contribution to this relative shift is easily calculated and given by

$$\frac{\Delta\nu_{dip}}{\nu_0} = -S_f \chi_{para} \tag{19}$$

where the factor S_f depends on the sample form and is $S_f \cong -4.1$ for a typical NMR thin cylindrical tube with a ratio (height/diameter) $\cong 10$. The susceptibility per volume unit χ_{para} of the paramagnetic solutes is $\chi_{para} = N_S g_S^2 \mu_B^2 S(S+1)/(3k_B T)$. For the free-radical spins studied, for which $S = 1/2$ and $g_S = 2$, we have

$$\frac{\Delta\nu_{dip}}{\nu_0} = 1.54 \times 10^{-3} \frac{c_S}{T} \tag{20}$$

The hyperfine scalar coupling is a short-ranged interaction that induces a relative frequency shift independent of the sample shape. For an electronic spin $S = 1/2$, it is given by

$$\frac{\Delta\nu_{hyp}}{\nu_0} = -\frac{1}{4} \frac{\gamma_I}{\gamma_S} \hbar \frac{\overline{A(r)}}{k_B T} = -\frac{1}{4} \frac{\hbar^2 \gamma_S^2}{b^3 k_B T} \overline{a(r)} \tag{21}$$

where $\overline{a(r)}$ is an average over the equilibrium pair distribution function $g_{IS}(R)$. The function $a(r)$ is commonly taken to be proportional to an exponential factor $\exp(-\lambda_s r)$, which describes the short-range decay of the ground-state electronic wave function and consequently of the free-electron density at a distance r from its mean position. Here, we assume that $a(r) = (c/r)\exp(-\lambda_s r)$, where the factor $1/r$ is introduced for mathematical convenience. We can expect a value of λ_s of the order of 1 Å^{-1}, while the factor $1/r$ has a much slower decrease than the exponential and has no physical importance. Now, we have all the necessary ingredients for interpretating the experimental frequency shifts.

Theoretical description of the ionic solutions in water

Solution model

Each water (w) molecule is modeled by a hard sphere of diameter $d_w = 2.8$ Å, with an embedded central polarizable electric dipole and a tetrahedral electric quadrupole [3]. The dipole, quadrupole. and

dipolar polarizability have their experimental values. The ions considered here are rather symmetric and are approximated as hard spheres.

Ion–ion potential of mean force

Our model of liquid solution is a mixture of hard spheres with embedded electric multipoles. Then, in the framework of the MOZ theory, the spatial correlations between the molecules can be taken into account more precisely by using reference closures, i.e., by approximating the bridge functions in the model of electrolyte solution by their counterparts in the mixture of neutral hard spheres of the same composition [16,18]. Our solutions contain small or moderate finite concentrations (FC) of the various ions. Then, the potential of mean force (PMF) w_{IS}^{FC} of the interacting ions can be derived from its infinite dilution limit w_{IS}^{ID} [20] within the Debye–Hückel (DH) limit, as follows [16,18]. On the one hand, to calculate the water–water spatial correlations, the simple reference linearized HNC (RLHNC) approximation is used, since it leads at 25 °C to a theoretical dielectric constant of pure water $\varepsilon = 77.5$ that compares favorably with the experimental value 78.5. This ensures an accurate treatment of the long-range Coulomb forces between the ions. The ion–water spatial correlations are also computed using the RLHNC approximation. On the other hand, the infinite dilution ion–ion PMF w_{IS}^{ID} is obtained within the more accurate reference HNC (RHNC) approximation from its straightforward expression in terms of the ion–ion indirect correlation function η_{IS}. The Debye–Hückel expression of $w_{IS}^{\mathrm{FC}}(R)$ for the ions M_I and M_S, of charges $q_I = z_I e$ and $q_S = z_S e$, reads

$$w_{IS}^{\mathrm{FC}}(R) = \begin{cases} \left[w_{IS}^{\mathrm{ID}}(R) - \dfrac{q_I q_S}{\varepsilon R} \right] + \dfrac{q_I q_S}{\varepsilon R} \dfrac{\exp[-\kappa(R-b)]}{(1+\kappa b)} & \text{if } R < b \\ \infty & \text{if } R \geq b \end{cases} \tag{22}$$

The inverse κ of the Debye length is given in CGS units by

$$\kappa = \left(\frac{8\pi e^2 \hat{I} N_{\mathrm{Avogadro}}}{1000 k_{\mathrm{B}} T \varepsilon} \right)^{1/2} \tag{23}$$

with the ionic strength $\hat{I} = \frac{1}{2} \sum_i c_i z_i^2$, the summation running over all ionic species i of concentrations c_i in mol.L^{-1}.

Diffusion coefficients

The MOZ theory only provides structural properties at equilibrium. The translational and rotational diffusion coefficients D^{t} and D^{r} have to be derived from experiment. For instance, the self-diffusion coefficients D^{t} can be measured by NMR pulsed magnetic field gradient (PMFG) techniques [14,18] or tracer methods.

Dynamic behavior of the ion pair $(CH_3)_4P^+/{}^{\bullet}ON(SO_3)_2^{2-}$ in D_2O solution by ^1H and ^{31}P NMR relaxation

We have investigated [15–18] the relative dynamics of the paramagnetic nitrosodisulfonate anion ${}^{\bullet}ON(SO_3)_2^{2-}$ (NDS^{2-}) with respect to the tetramethyl-phosphonium cation $(CH_3)_4P^+$ (TMP^+) in dilute D_2O solutions at 25 °C. We have measured the intermolecular longitudinal relaxation rates $R_{\mathrm{ln}}^{\mathrm{e}}$ of the $(CH_3)_4P^+$ protons and phosphorous nuclei, due to their magnetic coupling with the ${}^{\bullet}ON(SO_3)_2^{2-}$ electronic spins for several ionic strengths and resonance frequencies. In Fig. 4, the PMF $\beta w_{IS}^{\mathrm{FC}}$ of the TMP^+/NDS^{2-} pair is plotted for typical values of the screening parameter κd_w and the related theoretical dipolar relaxivities $(1/T_{i\mathrm{dip}}^{\mathrm{inter}})/c_S$ vs. κd_w are compared with the measured values $r_{\mathrm{ln}}^{\mathrm{e}} = R_{\mathrm{ln}}^{\mathrm{e}}/c_S$. For the three considered frequencies the agreement is quite satisfactory for the ^1H nuclei. This is a very encouraging result because there are no arbitrarily adjustable parameters in the theory. On the other hand, for the ^{31}P nuclei, the measured intermolecular relaxation process cannot be explained with-

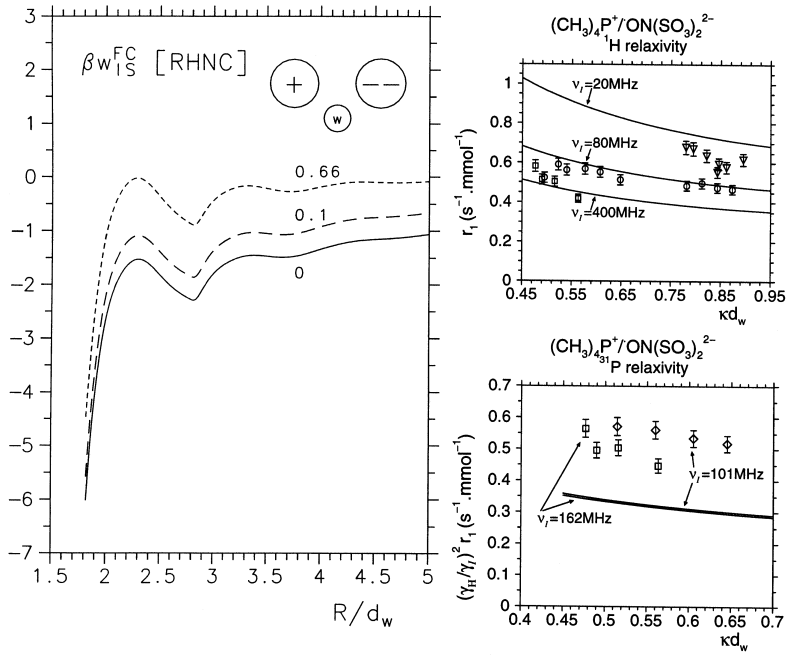

Fig. 4 (a) Influence of the screening parameter $\kappa d_w = 0$, 0.1, 0.66 on the $(CH_3)_4P^+/^{\bullet}ON(SO_3)_2^{2-}$ potential of mean force βw_{IS}^{FC} in water. (b) The ^{1}H relaxivity r_1 of the $(CH_3)_4P^+$ ion (experimental values at the ^{1}H resonance frequencies of 20, 80, and 400 MHz are shown by triangledowns, circles, and squares, respectively); the scaled ^{31}P relaxivity $(\frac{\gamma H}{\gamma I})^2 r_1$ of the $(CH_3)_4P^+$ ion, where γ_1 is the gyromagnetic ratio of the ^{31}P nuclear spin I (experimental values at the ^{31}P resonance frequencies of 101, 162 MHz are shown by diamonds and squares, respectively).

in our model for the relative distribution and motion of the pair TMP^+/NDS^{2-}, since the dipolar relaxivity can be 30% smaller.

Does the difference between the experimental relaxivity of the ^{31}P nuclei and its theoretical dipolar counterpart come from some failure of the above liquid model (imprecise values of the geometrical parameters, inaccuracy of the mean force potential, stochastic independence of the translational and rotational ionic motions) or from the neglect of the relaxation mechanism due to the hyperfine scalar coupling? To answer this question, in Fig. 5, we report the relative ^{1}H and ^{31}P experimental frequency shifts vs. the free-radical concentrations together with the theoretical expression (20) of the dipolar shift. For the protons, the perfect agreement between the experimental and theoretical values of the shifts shows that there is no measurable hyperfine scalar coupling. On the other hand, it is easily seen that the experimental relative shifts (18) for the ^{31}P nuclei at 298 K are about 3 times larger than the dipolar shifts calculated from eq. 20. This proves the existence of an important hyperfine coupling between a ^{31}P nucleus and a free-radical magnetic electron. From our theoretical expression (21), by using a reasonable value $\lambda_S b = 5$, we determined a value $c/b = -29$ of the hyperfine coupling coefficient through a mean square fit. For an average value of $\kappa d_w = 0.5$, typical of our solutions, we obtain, in first approximation, $\overline{A(r)} = 1.0 \times 10^6 c_S$ rad.s^{-1} or $\overline{a(r)} = -0.67 c_S$ rad.s^{-1}. These values are relevant because they are independent of the shape of the hyperfine coupling $a(r) = (c/r)\exp(-\lambda_s r)$ and consequently of the $\lambda_s b$ value. We also checked that when varying $\lambda_s b$ between 3 and 10, the values of c/b are modified without altering the quality of the $\Delta\nu/\nu_0$ fit.

The ^{31}P hyperfine coupling function $(a)r$ just determined in the framework of the diffusion model for spherical ions provides a negligible scalar hyperfine contribution $1/T_{1s}^{inter}$ to the expression (6) of

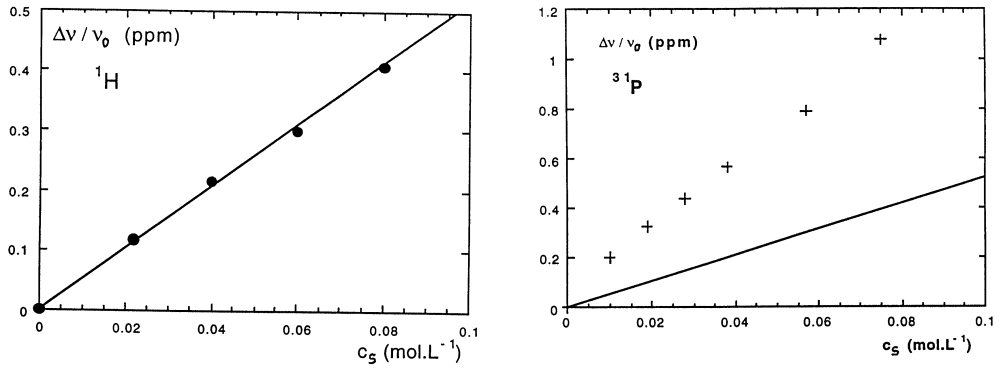

Fig. 5 Comparison between the observed relative frequency shifts of the ^{1}H and ^{31}P nuclei of the $(CH_3)_4P^+$ ion and the theoretical dipolar contributions to these shifts.

$1/T_1^{\text{inter}}$ at our rather high working magnetic fields B_0. Indeed, $\omega_S\tau \gg 1$ and $j_s(\omega_S)$, which decreases as ω_S increases, is very small, so that $1/T_{1s}^{\text{inter}} \propto j_s(\omega_S)$ can be neglected. The discrepancy observed for the ^{31}P relaxation rates is probably due to the strongly anisotropic collisional process between the attractive ions of the pair. The TMP^+ cation has tetrahedral symmetry, and the NDS^{2-} is approximately ellipsoidal in shape. Then, shorter minimal distances of approach between the ^{31}P nucleus and the free electron will be favored with respect to the hard-sphere model for some relative orientations of the ions.

For $B_0 \geq 4$T, the hyperfine coupling has a negligible effect on the longitudinal relaxation rate $1/T_1^{\text{inter}}$, which is governed by the magnetic dipolar intermolecular coupling. On the other hand, it significantly contributes to the transverse relaxation rate $1/T_2^{\text{inter}}$, because $1/T_{2s}^{\text{inter}}$ depends on the notable value $j_s(\omega_S = 0)$ of the scalar spectral density according to eq. 17. Both the T_1 and T_2 relaxation times of the ^{31}P nuclei were measured at $\nu_I = 81$ MHz ($B_0 = 4.7$ T) for various solutions of small and moderate ionic strengths. The ratio $T_1^{\text{inter}}/T_2^{\text{inter}}$ was found to have experimental values ≃1.53 in excellent agreement with their theoretical counterparts, provided that the hyperfine contribution is taken into account. On the other hand, for a purely dipolar relaxation mechanism, $T_{1\text{dip}}^{\text{inter}}/T_{2\text{dip}}^{\text{inter}} = 1.16$. This shows the overall validity of our theory for describing the dynamical properties of water with semi-dilute attractive ions. Accurate theoretical predictions are possible for $T_1^{\text{inter}}/T_2^{\text{inter}}$ because this ratio is much less sensitive than $1/T_1^{\text{inter}}$ and $1/T_2^{\text{inter}}$ to the inaccuracy of the model of the TMP^+/NDS^{2-} collision dynamics.

Intermolecular relaxation dispersion of the $(CH_3)_4N^+$ protons in Gd^{3+} heavy water solutions

Because paramagnetic gadolinium Gd^{3+} ions carry "pure" electronic spins of exceptionally high value $S = 7/2$, their clinically approved chelates are placed right in the middle of a revolutionary development in medical diagnostics [21]. Indeed, they enhance the relaxation rates of the protons of the surrounding water, so that they can increase the relaxation contrast between normal and diseased tissue in medical MRI. At the MRI fields $B_0 \approx 1$T, the nuclear relaxation induced by Gd^{3+} complexes depends on the longitudinal relaxation time T_{1e} of their electronic spins, which is too short for direct measurement and still needs an improved theoretical description. In order to help to characterize the efficiency of Gd^{3+} contrast agents, we present a typical NMRD study of the protons of tetramethylammonium $(CH_3)_4N^+$ (TMA^+) probe ions in D_2O solutions of $Gd(D_2O)_8^{3+}$ octoaqua ions at 298 K.

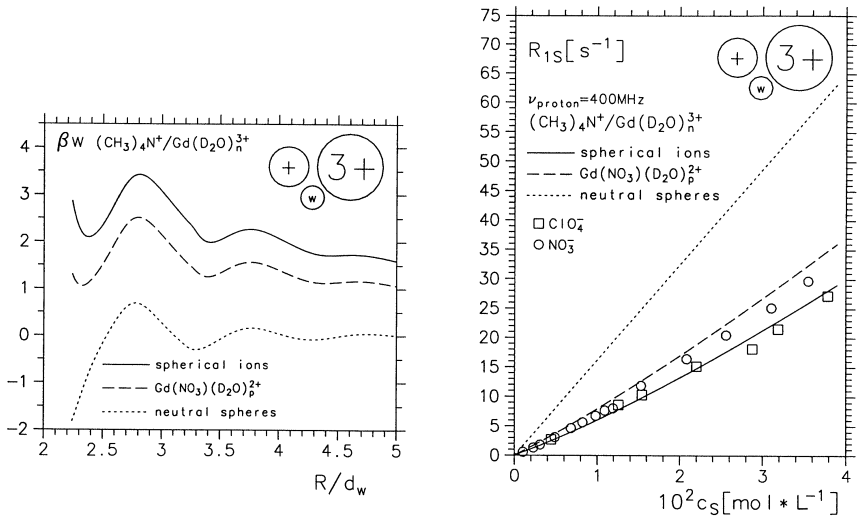

Fig. 6 (a) Various models for the $(CH_3)_4N^+/(Gd^{3+}$ aqua complex) potential of mean force β_w in water. (b) Comparison between the predicted intermolecular relaxation rates R_{1S} and the experimental values in the case of non complexing ClO_4^- anions and complexing NO_3^- anions in D_2O.

As a first step, we have performed relaxation measurements at 400 MHz (B_0 = 9.4T) [22] and above to assess the $TMA^+/Gd(D_2O)_8^{3+}$ relative dynamics. At these high NMR frequencies, $T_{1e} \geq 10^{-8}$ s for Gd^{3+}. As T_{1e} is much longer than the translational correlation time $\tau \approx 3 \times 10^{-10}$ s of the interionic motion, the longitudinal electronic relaxation is slow with respect to the ion–ion dynamics and its effects on the nuclear relaxation are negligible. We can use the Solomon relaxation expression (7) to calculate $R_{1S} = 1/T_{1dip}^{inter}$. In Fig. 6, various models for the PMF of the interacting ions are displayed. We also report the values of this dipolar relaxation rate for various Gd^{3+} concentrations in $Gd(ClO_4)_3$ solutions that only contain the noncomplexing ClO_4^- anions. The theoretical values, represented by a continuous line, are in excellent agreement with the experimental rates shown as white squares. The increasing slopes of the theoretical and experimental rates with c_S originate from the Debye–Hückel screening of the Coulomb repulsion between the studied ions. It should be pointed out that no adjustable parameter has been used in the theoretical model. We have also calculated the rates R_{1S} of a simple model of solution where the interacting ions are considered as neutral hard spheres in nonpolar water, also made of discrete hard spheres. The predicted values for the neutral spheres, represented by a dotted line, are more than twice as large as the experimental ones. This is a striking proof of the importance of Coulomb repulsion on the dynamical behavior of the ion pair.

For various concentrations of gadolinium nitrate $Gd(NO_3)_3$ we have also investigated the relaxation rates $R_{1S}(NO_3^-)$ of the TMA^+ protons. The experimental results are shown as white circles in Fig. 6, where they can be compared to the values $R_{1S}(ClO_4^-)$, which have been measured in the $Gd(ClO_4)_3$ solutions and previously discussed. The experimental rates in the presence of the NO_3^- ions are significantly larger than the corresponding values relative to the ClO_4^- solutions, especially as the Gd^{3+} concentration increases. This can be explained as follows. As the $Gd(NO_3)_3$ concentration increases, a negative complexing NO_3^- counterion can replace one or two water molecules of the first hydration shell of a rising percentage of the $Gd(D_2O)_8^{3+}$ ions. The newly formed species $Gd(NO_3)(D_2O)_p^{2+}$ carry smaller electric charges +2, instead of +3 for the $Gd(D_2O)_8^{3+}$ ions. They are less repelled by a TMA^+ cation. The Gd^{3+} paramagnetic centers are near the TMA^+ more often, which yields an increase of the dipolar coupling that induces the relaxation.

In order to study the complexation of the Gd^{3+} ions by the nitrates, it is useful to compute $R_{1S}(NO_3^-)$ for a simple model, in which all the purely hydrated ions $Gd(D_2O)_8^{3+}$ are replaced by $Gd(NO_3)(D_2O)_p^{2+}$ complexes, which are assumed to have the same spherical shape, diameter and self-diffusion constant, but which carry charges +2 instead of +3. Under these hypotheses, the calculated rate $R_{1S}(NO_3^-)$ of the TMA^+ protons due to the $Gd(NO_3)(D_2O)_p^{2+}$ cations is represented by the dashed curve in Fig 6b. It is slightly larger than the experimental rate $R_{1S}(NO_3^-)_{exp}$ at a given Gd^{3+} concentration. This can be interpreted by a chemical equilibrium

$$Gd(D_2O)_8^{3+} + NO_{3(aq)}^- \rightleftarrows Gd(NO_3)(D_2O)_p^{2+} \tag{24}$$

between the two gadolinium complexes, with a reasonable apparent equilibrium constant $K_{app} = 11.8\ L.mol^{-1}$. The same model of interionic motion could then successfully explain the measured relaxation rates R_{1S} at 400, 600, and 800 MHz in two D_2O solutions containing 0.1 M and 0.5 M of $(CH_3)_4N^+Cl^-$ and $\simeq 3 \times 10^{-3}$ M of $Gd(D_2O)_8^{3+}$. This confirms the negligible role of the electronic relaxation of the Gd^{3+} ion at these high NMR frequencies.

The second step of the NMRD probe solute method is a relaxation study, in which the field B_0 takes moderate values such as those used in MRI. Then, $R_{1n}^e = R_{1S}$ is sensitive to the electronic relaxation. For $0.23T \leq B_0 \leq 18.5T$ (10 MHz $\leq \nu_1 \leq$ 800 MHz), we measured [23] the rates $R_{1n}^e = R_{1S}$ of the TMA^+ protons in a dilute 0.1 M solution of TMA^+ in D_2O containing 3.08×10^{-3} M of Gd^{3+}. As the field $B_0 \to 0$, $\omega_I\tau$ decreases, whereas τ/T_{1e} increases, so that τ/T_{1e} cannot be neglected with respect to $\omega_I\tau$. Thus, the NMRD of protons requires a detailed knowledge of the electronic relaxation of the Gd^{3+} ion. For this purpose, we have undertaken a careful analysis [24] of the $Gd(D_2O)_8^{3+}$ EPR spectra measured by the Merbach group at various temperatures and fields. We have shown that, contrary to the usual assumption, the electronic relaxation is not only due to the effects of the transient zero-field splitting, but is also strongly influenced by the effects of the mean crystal field, which is static in the molecular frame. The static crystal field is modulated by the random Brownian rotation of the complex of rotational diffusion constant D_R. This motion is characterized by a rotational correlation time $\tau_R = 1/D_R = 1.95 \times 10^{-10}$s at $T = 298$ K. Our model allowed us to deduce the field dependence of the electronic relaxation functions. The longitudinal electronic relaxation function $k_{zz}(t)$ is well approximated using a single relaxation time, whereas the transverse electronic relaxation function is a superposition of four decreasing exponentials.

It is quite reasonable to suppose that the spatial molecular diffusion and the motion of the electronic spin are uncorrelated. Then, the correlation function $C_{zz}(t)$, which is relevant to the nucleus-electron dipole–dipole interaction, is simply the product

$$C_{zz}(t) = g_2(t)k_{zz}(t) \tag{25}$$

of the dipolar correlation function $g_2(t)$ defined by eq. 10 and of the longitudinal electronic relaxation function $k_{zz}(t) = (1/3)S(S+1)\exp(-|t|/T_{1e})$. We are now in a position to give the general expression for the theoretical intermolecular dipolar nuclear-electron relaxation rate R_{1n}^e due to the fluctuating electronic spins. Define the spectral density $j_2(\omega, 1/T_{1e})$ by

$$j_2(\omega, 1/T_{1e}) = \frac{1}{2\pi}\int_{-\infty}^{+\infty} g_2(t)\exp\left(-i\omega t - |t|/T_{1e}\right)dt \tag{26}$$

The new Solomon–Bloembergen (SB) type expression of R_{1n}^e, which should be used instead of eq. 7, reads after replacing γ_S by $-g_S\mu_B/\hbar$

$$R_{1n}^{e\,SB} = \frac{1}{T_{1dip}^{inter}} = \frac{8\pi^2}{5}\gamma_I^2(g_S\mu_B)^2\, j_2(\omega_I, 1/T_{1e}) \tag{27}$$

where the four spectral densities at the electronic frequency ω_S are dropped in this brief report, since they play a minor role for $B_0 \geq 0.5T$.

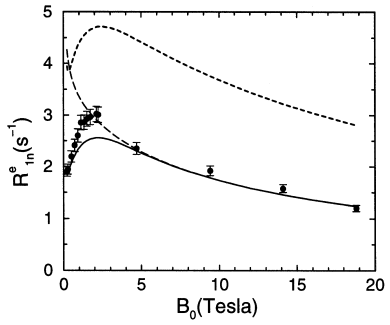

Fig. 7 ^{1}H NMRD profile for the $(CH_3)_4N^+/Gd(D_2O)_8^{3+}$ ion pair in D_2O. The predictions of models (i), (ii), and (iii) are represented by continuous, long-dashed, and dashed lines, respectively.

In Fig. 7, the experimental NMRD data are compared to the theoretical predictions of three different models. Model i incorporates the influence of the Coulomb repulsion of the PMF given by eq. 22 on the ion–ion relative diffusion. Model ii accounts for the repulsive ion–ion PMF as in model i, but neglects all of the effects of the electronic relaxation by using the Solomon eq. 7. Finally, model iii describes the ion–ion relative diffusion as that of neutral hard spheres in a viscous continuum and assumes that the spins are located at the ion centers.

With the most realistic model i, the overall agreement is good for all of the investigated fields, and in particular, the position of the maximum at $B_0 \simeq 2.2$T is well predicted. The theoretical predictions are excellent at high fields >4T, where the electronic relaxation effects vanish so that the Solomon eq. 3 applies. This justifies the model of interionic dynamics. The theoretical values are slightly lower than the experimental data at low fields, but the discrepancy never exceeds ~15%. This is quite remarkable because there are no adjustable parameters and because the NMR experimental accuracy is of the order of 5%.

To our knowledge, this is the first time that an electronic relaxation model of the Gd^{3+} ion, with convenient parameters for the underlying physical processes, is able to interpret the EPR line widths at various temperatures and fields and that the same set of parameters accounts, in a reasonably accurate way, for the effect of the fast electronic relaxation on the proton magnetic relaxation dispersion due to the translational encounters of the cation/Gd^{3+} pairs.

For completeness, now consider the $R^e_{1n} = R_{1S}$ predictions of models ii and iii, also represented in Fig. 7. The smaller results of model i (continuous curve) with respect to the values of model ii (long-dashed curve) display the influence of the electronic relaxation on the NMRD profile for $B_0 < 4$T. At $B_0 = 0.5$T which is the MRI field of reference, the TMA^+ proton relaxation rate R^e_{1n} is decreased by ~50% because of the short value of T_{1e} with respect to the translational correlation time τ. The smaller values of model i (and of model ii) with respect to the predictions of model iii (dashed line) indicate the marked influence of the Coulomb repulsion on the spatial relative dynamics of the $TMA^+/Gd(D_2O)_8^{3+}$ ion pair. This electrostatic repulsion is in no way negligible, leading to a reduction of R^e_{1n} by a factor of ≈2.

Here, we have used an independent EPR study to infer the longitudinal electronic relaxation time T_{1e} needed to interpret the NMRD profile. The reverse procedure is also useful. NMRD experiments, using probe solutes of well-known spatial dynamics with respect to a Gd^{3+} complex, can be combined with the new Solomon–Bloembergen equation (27) to provide an indirect estimate of T_{1e} in this complex. In our case, the values of T_{1e} through this procedure are in good agreement with those derived from the analysis of the EPR data.

DISCUSSION

Integral equation (IE) theories of the statistical mechanics of liquids, such as the MOZ-HNC approximation and its derivatives applied in this article, only yield approximate properties at equilibrium. However, the examples given, ranging from pure aprotic solvents to electrolyte solutions of dissociated ions, demonstrate their accuracy and even their ability to predict dynamical properties in the framework of Brownian diffusion. Moreover, they deliver liquid properties without any statistical bias [25] or noise and within computer times that can be orders of magnitude shorter than those needed by simulations. For instance, computing a whole intermolecular NMRD profile in a paramagnetic aqueous solution of several different spherical ions requires only a minute on a modern workstation! Therefore, they enable us to determine the unknown parameters of interaction models through the fitting of theoretical results to their experimental counterparts.

IE theories have also been successful in many other areas, including the solvation thermodynamics in electrolyte solutions [1,26–28], the description of liquid–gas phase transitions [29], transport properties of ions [30], colloid systems [31], or chiral fluids [32] using a diagrammatically correct site–site method [33]. In view of these successes, continuous effort has been devoted to remedy the weaknesses of the IE theories. On the one hand, to improve upon the HNC approximation, more accurate bridge functions $B_{AB}(12)$ have been proposed for systems of neutral hard spheres [34], of spherical ions [35], and for many fluids of anisotropic molecules [36]. An alternative route to deal with liquids of associating molecules such as water, in which the bridge term plays a notable role [37], was pioneered by Wertheim [38,39], who suggested to treat the excluded volume effects on association by replacing the usual OZ theory by a new formalism. For instance, this Wertheim OZ (WOZ) theory already led to encouraging results for electrolyte solutions with strong anion-cation association [40] and for H-bonded hydrogen fluoride [41]. On the other hand, the IE theories, which initially were developed to deal with molecules without internal degrees of freedom, have been extended to account for the important molecular polarizability, either by employing effective partial charges and electric dipoles [3,42] or by extending the conventional OZ approach to a more general IE formalism [43].

About 50 years ago, Eugene Wigner stated [44]: "With statistical mechanics, we can calculate (almost) nothing—exactly". The theory of intermolecular NMRD in paramagnetic solutions [45], which combines classical theory of the liquid state and quantum theory of irreversible processes, is clearly a domain of chemical thermodynamics where this pessimistic comment is no longer valid. Until now, the application of IE theories to solutions in nonaqueous solvents has been rather restricted. Now, very numerous studies, including systematic careful experiments and physical models, have already been published on these systems by Hertz *et al*. [13,14,46] and Barthel *et al.* [1]. It will certainly be rewarding to revisit this considerable work in the light of the recent development of liquid-state theory and, when necessary, to complete it by additional studies using the very promising high-resolution NMRD technique at low and intermediate fields [47].

REFERENCES

1. J. M. G. Barthel, H. Krienke, W. Kunz. *Physical Chemistry of Electrolyte Solutions. Modern Aspects*, Springer, Darmstadt (1998).
2. L. Blum and A. J. Torruella. *J. Chem. Phys.* **56**, 303 (1972).
3. S. L. Carnie and G. N. Patey. *Mol. Phys.* **47**, 1129 (1982).
4. P. H. Fries and G. N. Patey. *J. Chem. Phys.* **82**, 429 (1985).
5. F. Lado, M. Lombardero, E. Enciso, S. Lago, J. L. F. Abascal. *J. Chem. Phys.* **85**, 2916 (1986).
6. P. H. Fries, W. Kunz, P. Calmettes, P. Turq. *J. Chem. Phys.* **101**, 554 (1994).
7. J. Richardi, P. H. Fries, R. Fischer, S. Rast, H. Krienke. *J. Mol. Liq.* **73**, 465 (1997).
8. J. Richardi, P. H. Fries, R. Fischer, S. Rast, H. Krienke. *Mol. Phys.* **93**, 925 (1998).
9. J. Richardi, P. H. Fries, H. Krienke. *J. Chem. Phys.* **108**, 4079 (1998).

10. P. T. Cummings and G. Stell. *Mol. Phys.* **46**, 383 (1982).
11. H. Bertagnolli, P. Chieux, M. D. Zeidler. *Mol. Phys.* **32**, 759 (1976).
12. H. C. Torrrey. *Phys. Rev.* **92**, 962 (1953).
13. M. Holz. *Progr. NMR Spectrosc.* **18**, 327 (1986).
14. A. Sacco. *Chem. Soc. Rev.* **23**, 129 (1994).
15. (a) P. Fries, E. Belorizky. *J. Phys. Paris* **39**, 1263 (1978); (b) P. H. Fries, G. N. Patey. *J. Chem. Phys.* **80**, 6253 (1984); (c) P. H. Fries, E. Belorizky, J. C. T. Rendell, E. E. Burnell, G. N. Patey. *J. Phys. Chem.* **94**, 6263 (1990).
16. M. Jeannin, E. Belorizky, P. H. Fries, W. Gorecki. *J. Phys. II France* **3**, 1511 (1993).
17. E. Belorizky, P. H. Fries, W. Gorecki, M. Jeannin, C. Roby. *J. Phys. Chem.* **98**, 4517 (1994).
18. A. Sacco, E. Belorizky, M. Jeannin, W. Gorecki, P. H. Fries. *J. Phys. II France* **7**, 1299 (1997).
19. E. Belorizky, P. H. Fries, W. Gorecki, M. Jeannin. *J. Phys. II France* **1**, 527 (1991).
20. E. Guàrdia, R. Rey, J. A. Padró. *J. Chem. Phys.* **95**, 2823 (1991).
21. P. Caravan, J. J. Ellison, T. J. McMurry, R. B. Lauffer. *Chem. Rev.* **99**, 2293 (1999).
22. C. Vigouroux, M. Bardet, E. Belorizky, P. H. Fries, A. Guillermo. *Chem. Phys. Lett.* **286**, 93 (1998).
23. S. Rast, E. Belorizky, P. H. Fries, J. P. Travers. *J. Phys. Chem B* **105**, 1978 (2001).
24. S. Rast, A. Borel, L. Helm, E. Belorizky, P. H. Fries, A. E. Merbach. *J. Am. Chem. Soc.* **123**, 2637 (2001).
25. J. M. Caillol, D. Levesque, J. J. Weis. *Mol. Phys.* **69**, 199 (1990).
26. P. G. Kusalik and G. N. Patey. *J. Chem. Phys.* **88**, 7715 (1988).
27. D. Beglov and B. Roux. *J. Chem. Phys.* **104**, 8678 (1996).
28. A. A. Chialvo, P. T. Cummings, J. M. Simonson, R. E. Mesmer. *J. Chem. Phys.* **110**, 1075 (1999).
29. J. A. Anta, E. Lomba, M. Alvarez, M. Lombardero, C. Martín. *J. Phys. Chem. B* **101**, 1451 (1997).
30. O. Bernard, W. Kunz, P. Turq, L. Blum. *J. Phys. Chem.* **96**, 3834 (1992).
31. O. Spalla and L. Belloni. *Phys. Rev. Lett.* **74**, 2515 (1995).
32. N. M. Cann and B. Das. *J. Chem. Phys.* **113**, 2369 (2000).
33. D. Chandler, R. Silbey, B. M. Ladanyi. *Mol. Phys.* **46**, 1335 (1982).
34. P. Attard and G. N. Patey. *J. Chem. Phys.* **92**, 4970 (1990).
35. R. Bacquet and P. J. Rossky. *J. Chem. Phys.* **79**, 1419 (1983).
36. J. A. Anta, E. Lomba, M. Alvarez, C. Martín, M. Lombardero. *J. Chem. Phys.* **106**, 2712 (1997).
37. M. Lombardero, C. Martín, S. Jorge, F. Lado, E. Lomba. *J. Chem. Phys.* **110**, 1148 (1999).
38. M. S. Wertheim. *J. Stat. Phys.* **42**, 459 (1986).
39. M. S. Wertheim. *J. Stat. Phys.* **42**, 477 (1986).
40. Yu. V. Kalyuzhnyi, M. F. Holovko, A. D. J. Haymet. *J. Chem. Phys.* **95**, 9151 (1991).
41. P. H. Fries and J. Richardi. *J. Chem. Phys.* **113**, 9169 (2000).
42. J. Richardi, P. H. Fries, J. C. Soetens. *J. Mol. Liq.* **88**, 209 (2000).
43. F. Lado, E. Lomba, M. Lombardero. *J. Chem. Phys.* **108**, 4530 (1998).
44. J. M. Prausnitz. *Pure Appl. Chem.* **72**, 1819 (2000).
45. E. Belorizky, P. H. Fries, S. Rast. *C. R. Acad. Sci. Paris, Chimie* **4**, 825 (2001).
46. M. D. Zeidler. *Mol. Phys.* **30**, 1441 (1975).
47. S. Wagner, T. R. J. Dinesen, T. Rayner, R. G. Bryant. *J. Magn. Reson.* **140**, 172 (1999).